

# Trustworthy Evaluation of Generative AI Models

Zijun Gao\* Yan Sun†

February 3, 2025

## Abstract

Generative AI (GenAI) models have recently achieved remarkable empirical performance in various applications, however, their evaluations yet lack uncertainty quantification. In this paper, we propose a method to compare two generative models based on an unbiased estimator of their relative performance gap. Statistically, our estimator achieves parametric convergence rate and asymptotic normality, which enables valid inference. Computationally, our method is efficient and can be accelerated by parallel computing and leveraging pre-storing intermediate results. On simulated datasets with known ground truth, we show our approach effectively controls type I error and achieves power comparable with commonly used metrics. Furthermore, we demonstrate the performance of our method in evaluating diffusion models on real image datasets with statistical confidence.

## 1 Introduction

Generative models have achieved remarkable success across numerous applications, showcasing their versatility and effectiveness in domains such as image synthesis, natural language processing, and scientific discovery (Achiam et al. 2023; Goodfellow et al. 2014; Karras et al. 2020; Van Den Oord et al. 2016). While extensive research has focused on developing and refining generative models, comparatively less attention has been given to evaluating these models. Evaluating generative models is essential for quantifying the quality of their outputs and identifying the best model when comparing multiple options.

Evaluating a generative model is significantly more challenging than the evaluation of a predictor or a classifier. To evaluate the performance of prediction or classification, we can directly compare the model’s output with the true label. In contrast, the quality of a generative model is determined by how closely the distribution of its generated data matches that of the input data, rather than the similarity between generated data points and input data points (also known as the reconstruction error). To make matters worse, generative models often produce high-dimensional outputs<sup>1</sup>. In papers of generative models, visually inspecting a few representative generated images are often used to argue that one approach outperforms another. Even though visual investigation can provide an intuitive comparison of generative models, this qualitative evaluation is inherently subjective, difficult to scale, and struggles to capture subtle discrepancies (Section 6.2). For quantitative metrics, the options are relatively limited (discussed further in Appendix A), with the Frechet Inception Distance (FID) (Heusel et al. 2017) being the most commonly used. However, FID cannot be computed exactly, and its approximation error heavily depends on the quality of the intermediate feature extractors and nuisance distribution estimators employed in the evaluation process.

In this paper, we propose a method for comparing and evaluating a wide range of generative models with uncertainty quantification. To our knowledge, this is the first framework to offer rigorous generative model comparison with statistical confidence. In details, we make the following contributions:

---

\*Marshall School of Business, University of Southern California, USA

†Wharton School of Business, University of Pennsylvania, USA

<sup>1</sup>The output is typically ultra-high-dimensional, for example, a 1080p resolution image consists of around  $2 \times 10^6$  pixels with (approximately) continuous value. Particularly, an image is represented as a matrix of size  $d_1 \times d_2$ , where  $d = d_1 \cdot d_2$  is the total number of pixels. Each pixel consists of three color channels (e.g., RGB), where each channel takes integer values ranging from 0 to 255. As a result, a single pixel can represent  $256^3 \approx 16.7 \times 10^6$  possible color combinations. The pixel values can effectively be regarded as continuous.

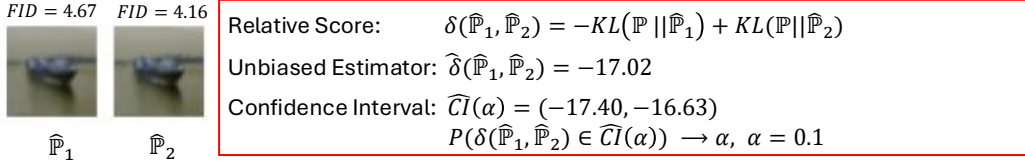


Figure 1: An example of our method applied to comparing the DDIM model with different numbers of denoising steps  $S$ . Here,  $\mathbb{P}$  represents the distribution of the test images,  $\hat{\mathbb{P}}_1$  corresponds to the DDIM model with  $S = 50$  denoising steps, and  $\hat{\mathbb{P}}_2$  corresponds to the DDIM model with  $S = 100$  denoising steps. Our method demonstrates that the confidence interval for the relative score  $\delta(\hat{\mathbb{P}}_1, \hat{\mathbb{P}}_2)$  is significantly negative, indicating that  $\hat{\mathbb{P}}_2$  with  $S = 100$  achieves significantly better performance. Our comparison is consistent with the FID provided in Song, Meng, and Ermon 2021.

- *Evaluation objective.* Instead of evaluating each generative model’s absolute performance separately, we focus on directly assessing the *relative* performance<sup>2</sup> between two generative models, which is sufficient for identifying the better one.
- *Statistical property.* For the relative score, we develop an *unbiased* estimator in the form of a first-order U-statistic that achieves convergence at the parametric rate. Additionally, we explicitly characterize the asymptotic distribution of our estimator, enabling the statistical inference of the relative score and the comparison of generative models with confidence.
- *Empirical performance.* On simulated datasets with known ground truth, we demonstrate that our approach constructs faithful confidence intervals, whereas existing estimators paired with resampling methods (e.g. bootstrap, subsampling) fail to achieve the correct coverage rate. Furthermore, we demonstrate the effectiveness of our method in evaluating diffusion models on real image datasets (CIFAR10). Our method aligns with existing metrics in assessing the relative performance of diffusion models, and it also enables drawing conclusions with statistical confidence (see Figure 1 for an example of our method applied to comparing the DDIM model with different number of denoising steps).

**Organization.** In Section 2, we review the standard generative model structure and formulate the problem of evaluating generative models. In Section 3, we introduce the concept of the relative score for comparing generative models and demonstrate how a key cancellation enables its estimation and inference. In Section 4, we present our estimator for the relative score, derive its asymptotic distribution, and detail the construction of the confidence intervals. In Section 5, we discuss the computation aspect of our method. In Section 6, we evaluate the numerical performance of our methods using both simulated and real datasets. We compare our method against other evaluation metrics regarding type I error control and statistical power. In Section 7, we conclude with directions for future research. All proofs are deferred to the Supplementary Materials.

**Notations.** Let  $\Omega$  denote the space of test data, and let  $\mathbb{P}$  represent the true target distribution. Let  $\hat{\mathbb{P}}_1$  denote the distribution of data generated by a generative model. If the generative process of the generative model involves sampling a random noise vector, we use  $d_1$  to denote the dimension of its dimension. Similarly we define  $\hat{\mathbb{P}}_2$  and  $d_2$ . Let  $\mathbb{P}_n$  represent the empirical distribution of  $n$  observations from  $\mathbb{P}$ , and similarly for  $\hat{\mathbb{P}}_{1,n}, \hat{\mathbb{P}}_{2,n}$ . We denote densities by lower-case letters, e.g.,  $p$  as the density of  $\mathbb{P}$ . In a generative model, for an invertible backward process  $g_1$ , we use  $g_1^{-1}$  to denote the inverse of  $g_1$  and let  $\mathbb{Q}_1$  and  $\hat{\mathbb{Q}}_1$  be the distributions of  $Z_1 = g_1^{-1}(Y)$  where  $Y \sim \mathbb{P}$  and  $Y \sim \hat{\mathbb{P}}_1$ , respectively. Let  $J_{g_1^{-1}}(y)$  be the Jacobian matrix of  $g_1^{-1}$  at  $y$ , and let  $|J_{g_1^{-1}}|(y)$  be its determinant<sup>3</sup>, and in a similar spirit we define  $J_{g_1}(z_1)$  and  $|J_{g_1}|(z_1)$ . We use  $\phi_d$  to

<sup>2</sup>For a generator, we use the KL divergence between the test data distribution and its output distribution as the absolute performance metric. The relative performance between two generators is then defined as the difference between their absolute scores.

<sup>3</sup>If  $J_{g_1^{-1}}(y)$  is not a square matrix, we define  $|J_{g_1^{-1}}|(y)$  as  $\max \left\{ \det \left( J_{g_1^{-1}}^\top(y) J_{g_1^{-1}}(y) \right)^{1/2}, \det \left( J_{g_1^{-1}}(y) J_{g_1^{-1}}^\top(y) \right)^{1/2} \right\}$ .

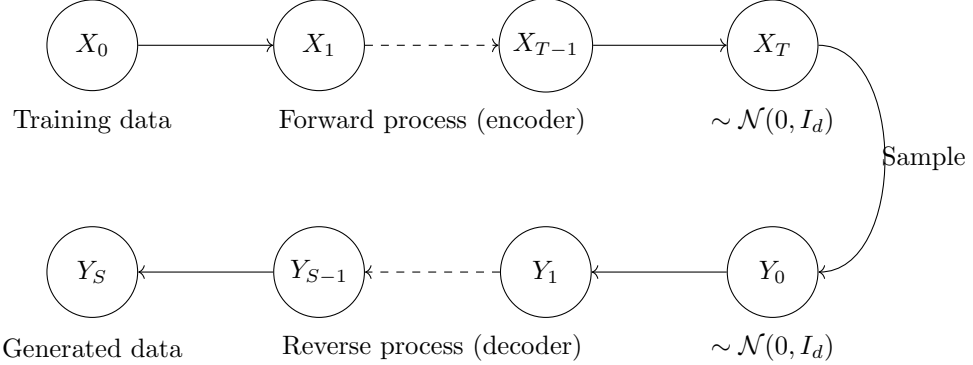


Figure 2: Forward and backward processes of a generative model.

denote the density of the standard multivariate Gaussian density in  $\mathbb{R}^d$ . For  $x \in \mathbb{R}^d$ , we use  $\|x\|$  to denote its  $\ell_2$  norm.

## 2 Background

### 2.1 Generative model

There is a vast body of literature on generative models, including variational auto-encoders (Kingma 2013), autoregressive models (Van Den Oord, Kalchbrenner, and Kavukcuoglu 2016), normalizing flows (Dinh, Sohl-Dickstein, and Bengio 2016; Rezende and Mohamed 2015), diffusion models (Ho, Jain, and Abbeel 2020; Song, Meng, and Ermon 2021; Song and Ermon 2019), to name a few. Many of these models, including all the aforementioned approaches, consist of a forward and a reverse process, as illustrated in Figure 2. In the forward process (encoder), data are progressively transformed (by neural networks, gradient flow, or adding noise) for multiple iterations, eventually converting the input data into a pure noise, typically following a multivariate Gaussian distribution. In the reverse process (decoder), a noise random variable is sampled and then gradually modified to construct a new data point.

Our comparison method is compatible with any generative model of the form in Figure 2 satisfying the following assumptions.

**Assumption 2.1.** *The noise distribution is known.*

As a convention, we adopt the standard multivariate Gaussian distribution as the noise distribution consistent with common practices in generative models.

**Assumption 2.2.** *The reverse process is invertible.*

For normalizing flows, the reverse process follows an ordinary differential equation (ODE) (Chen et al. 2018), which can be straightforwardly reverted by walking backwards in time. Similarly for the Denoising Diffusion Implicit Model (DDIM) (Song, Meng, and Ermon 2021), the reverse process is deterministic, which can be considered as the Euler method to solve an ODE, and inverting the process can be done by reverting the ODE. Although our theoretical framework assumes access to the exact inverse of the reverse process, our numerical experiments show that our methods produce valid inferences even when using a learned inverse, which can be achieved by commonly used generative models. For instance, we can train an auto-encoder on the data generated by  $g_1$ , and the encoder effectively serves as  $g_1^{-1}$  if the auto-encoder's reconstruction error is zero. See Section 6 for details.

### 2.2 Comparison of generative models

In this paper, we focus on the case where a set of  $n_{\text{test}}$  test data points  $Y_i$ ,  $1 \leq i \leq n_{\text{test}}$  independently and identically distributed (i.i.d.) from the target distribution  $\mathbb{P}$ , are provided. We aim to compare generative

models using the test dataset. For conciseness, we focus on the comparison of two models, denoted by  $\hat{\mathbb{P}}_1$  and  $\hat{\mathbb{P}}_2$ , while the generalization to multiple-model comparisons is straightforward and discussed in Section 7.

Generative models aim to approximate  $\mathbb{P}$ , with better performance indicated by greater similarity between  $\hat{\mathbb{P}}_1$  and  $\mathbb{P}$ . To evaluate a generative model quantitatively, a dissimilarity metric between  $\mathbb{P}$  and  $\hat{\mathbb{P}}_1$  is computed. In this work, we use the KL divergence, also known as relative entropy. Alternative dissimilarity metrics ( $f$ -divergence and Wasserstein distance) are discussed in Appendix A.

We first state the assumption of  $\mathbb{P}$  and  $\hat{\mathbb{P}}_1$  such that their KL-divergence is well-defined<sup>4</sup>.

**Assumption 2.3.** *Suppose the test data distribution  $\mathbb{P}$  and the generated data distribution  $\hat{\mathbb{P}}_1$  admit densities, and  $\mathbb{P}$  is absolutely continuous with respect to  $\hat{\mathbb{P}}_1$ .*

Under Assumption 2.3, we formally define the absolute score for the generative model<sup>5</sup> associated with  $\hat{\mathbb{P}}_1$  as the negative KL divergence between  $\mathbb{P}$  and  $\hat{\mathbb{P}}_1$ ,

$$s(\hat{\mathbb{P}}_1) := -\text{KL}(\mathbb{P} \parallel \hat{\mathbb{P}}_1) = - \int \log \left( \frac{p(y)}{\hat{p}_1(y)} \right) p(y) dy. \quad (1)$$

A larger absolute score  $s(\hat{\mathbb{P}}_1)$  indicates better performance of the generative model  $\hat{\mathbb{P}}_1$ .

### 3 Relative score for generative model comparison

Despite the popularity of KL-divergence (our absolute score), its estimation and inference are considerably challenging. According to (Zhao and Lai 2020), the minimax optimal rate for estimating the KL divergence between two densities in  $\mathbb{R}^d$ , based on a sample of size  $n_{\text{test}}$  from each density, scales as slow as  $n_{\text{test}}^{-2/d}$ . In addition, the asymptotic distribution of KL-divergence is typically intractable except for special cases (Belov and Armstrong 2011), and computationally-heavy bootstrap or subsampling methods are called for to conduct inference based on the KL-divergence (Arizono and Ohta 1989).

Instead of investigating the absolute scores of two generative models separately, we propose to directly study the relative score—the difference between their absolute scores defined as

$$\delta(\hat{\mathbb{P}}_1, \hat{\mathbb{P}}_2) := s(\hat{\mathbb{P}}_1) - s(\hat{\mathbb{P}}_2) = -\text{KL}(\mathbb{P} \parallel \hat{\mathbb{P}}_1) + \text{KL}(\mathbb{P} \parallel \hat{\mathbb{P}}_2). \quad (2)$$

The relative score aims to quantify the performance gap between the two generative models. If  $\delta(\hat{\mathbb{P}}_1, \hat{\mathbb{P}}_2) > 0$ , it implies that  $\text{KL}(\mathbb{P} \parallel \hat{\mathbb{P}}_1) < \text{KL}(\mathbb{P} \parallel \hat{\mathbb{P}}_2)$ , and we conclude that  $\hat{\mathbb{P}}_1$  is superior to  $\hat{\mathbb{P}}_2$ .

In contrast to the absolute score, the relative score benefits from a nice cancellation of some hard-to-estimate term, facilitating its estimation and inference. Explicitly, the absolute score (1) contains two terms, with  $\int \log(\log(p(y)) d\mathbb{P}(y)$  being less tractable than  $\int \hat{p}_1(y) d\mathbb{P}(y)$ , as the generating mechanism  $\hat{p}_1(y)$  is essentially known (Proposition 2). By the definition of the relative score (2),

$$\begin{aligned} \delta(\hat{\mathbb{P}}_1, \hat{\mathbb{P}}_2) &= - \left( \int \log(p(y)) d\mathbb{P}(y) - \int \log(\hat{p}_1(y)) d\mathbb{P}(y) \right) + \left( \int \log(p(y)) d\mathbb{P}(y) - \int \log(\hat{p}_2(y)) d\mathbb{P}(y) \right) \\ &= \int \log(\hat{p}_1(y)) d\mathbb{P}(y) - \int \log(\hat{p}_2(y)) d\mathbb{P}(y). \end{aligned} \quad (3)$$

Here the challenging-to-estimate term  $\int \log(p(y)) d\mathbb{P}(y)$ , appearing in both  $\text{KL}(\mathbb{P} \parallel \hat{\mathbb{P}}_1)$  and  $\text{KL}(\mathbb{P} \parallel \hat{\mathbb{P}}_2)$ , cancels out! The remaining term  $\int \log(\hat{p}_1(y)) - \log(\hat{p}_2(y)) d\mathbb{P}(y)$  is the expectation of an effectively known function  $\log(\hat{p}_1(y)) - \log(\hat{p}_2(y))$  regarding the test data distribution. Therefore, the relative score can be efficiently estimated using a first-order U-statistic based on a set of test data points, detailed in Section 4 below.

We conclude this section by showing that the attractive cancellation (3) in the relative score is unique to our choice of KL divergence. For a convex function  $f : [0, +\infty) \rightarrow (-\infty, +\infty]$  such that  $f(x)$  is finite

<sup>4</sup>In this paper, we focus on  $\mathbb{P}, \hat{\mathbb{P}}_1$  with continuous supports. For discrete-support distributions, we can replace the arguments below by their discrete analogue and arrive at similar results.

<sup>5</sup>For conciseness, we use the generating distribution to represent its corresponding generative model. For example, we may refer to the generative model as  $\hat{\mathbb{P}}_1$ .

for all  $x > 0$ ,  $f(1) = 0$ , and  $f(0) = \lim_{t \rightarrow 0^+} f(t)$ , the f-divergence of  $\mathbb{P}$  from  $\hat{\mathbb{P}}_1$  is defined as  $D_f(\mathbb{P} \parallel \hat{\mathbb{P}}_1) := \int_{\Omega} f\left(\frac{p(y)}{\hat{p}_1(y)}\right) \hat{p}_1(y) dy$ . KL-divergence is a special case of f-divergence with  $f(x) = x \log(x)$ .

**Proposition 1.** *For an f-divergence with  $f \in C^1$ , if there exists a function  $g$  such that for any  $\hat{\mathbb{P}}_1, \hat{\mathbb{P}}_2, \mathbb{P}$ ,*

$$D_f(\mathbb{P} \parallel \hat{\mathbb{P}}_1) - D_f(\mathbb{P} \parallel \hat{\mathbb{P}}_2) = \int g(\hat{\mathbb{P}}_1, \hat{\mathbb{P}}_2) d\mathbb{P}, \quad (4)$$

*then there exists  $\beta \geq 0$  such that  $f(x) = \beta x \log(x)$ , i.e.,  $D_f(\mathbb{P} \parallel \hat{\mathbb{P}}_1) = \beta KL(\mathbb{P} \parallel \hat{\mathbb{P}}_1)$ .*

We prove Proposition 1 by (1) reducing it to the Cauchy functional equation problem through multiple rounds of re-parametrization; (2) applying the uniqueness of the solution to the Cauchy functional equation. The detailed proof can be found in the Supplementary Materials.

## 4 Estimation and inference of relative score

In the following section, we focus on estimating the relative score and constructing confidence intervals for it using the simplified expression (3).

### 4.1 Estimation

In a generative model,  $g_1$  is known and accessible. Then  $\hat{p}_1(y)$  can be computed explicitly using the noise distribution and the change of measure. Recall that we consider the standard multivariate Gaussian distribution as the noise distribution, then we have the following proposition:

**Proposition 2.** *Under Assumption 2.1 and Assumption 2.2, the density  $\hat{p}_1(x)$  is given by*

$$\hat{p}_1(y) = \phi_{d_1}(g_1^{-1}(y)) \cdot |J_{g_1}(g_1^{-1}(y))|.$$

Combined with the simplified form (3), we estimate the relative score by the first-order U-statistic,

$$\hat{\delta}(\hat{\mathbb{P}}_1, \hat{\mathbb{P}}_2) := \frac{1}{n_{\text{test}}} \sum_{i=1}^{n_{\text{test}}} \log(\hat{p}_1(Y_i)) - \log(\hat{p}_2(Y_i)). \quad (5)$$

According to the standard property of U-statistics, we establish the following unbiasedness result.

**Proposition 3.** *The estimator  $\hat{\delta}(\hat{\mathbb{P}}_1, \hat{\mathbb{P}}_2)$  in (5) is unbiased, i.e.,  $\mathbb{E}[\hat{\delta}(\hat{\mathbb{P}}_1, \hat{\mathbb{P}}_2)] = \delta(\hat{\mathbb{P}}_1, \hat{\mathbb{P}}_2)$ .*

### 4.2 Inference

We describe the asymptotic distribution of the estimator in (5) in the following theorem.

**Theorem 4.1.** *Let  $V := \text{Var}(\log(\hat{p}_1(Y_i)) - \log(\hat{p}_2(Y_i)))$ . If  $V < \infty$ ,*

$$\sqrt{n_{\text{test}}} \left( \hat{\delta}(\hat{\mathbb{P}}_1, \hat{\mathbb{P}}_2) - \delta(\hat{\mathbb{P}}_1, \hat{\mathbb{P}}_2) \right) \xrightarrow{d} \mathcal{N}(0, V).$$

The detailed proof is provided in the appendix. If  $\mathbb{P}(\hat{p}_1(Y_i) \neq \hat{p}_2(Y_i)) > 0$ , then  $V > 0$ , and the asymptotic distribution is non-degenerate. If  $\hat{p}_1(Y_i)$  and  $\hat{p}_2(Y_i)$  are the same almost surely, then  $V = 0$ , and the asymptotic distribution becomes degenerate, supported at the point zero. However, the degenerate scenario is unlikely to occur, as two distinct generative models rarely agree with probability one.

By the law of large numbers, the empirical variance of  $\log(\hat{p}_1(Y_i)) - \log(\hat{p}_2(Y_i))$ , denoted by  $\hat{V}$ , is a consistent estimator of  $V$ . Using Slutsky's theorem (see e.g., Lemma 2.8 of Vaart 2000), we derive the following corollary of Theorem 4.1.

**Corollary 4.1.** *If  $0 < V < \infty$ , then*

$$\frac{\hat{\delta}(\hat{\mathbb{P}}_1, \hat{\mathbb{P}}_2) - \delta(\hat{\mathbb{P}}_1, \hat{\mathbb{P}}_2)}{\sqrt{\hat{V}/n_{test}}} \xrightarrow{d} \mathcal{N}(0, 1). \quad (6)$$

Corollary 4.1 allows us to perform statistical inference on the relative score, enabling the determination of the better generative model with a specified level of confidence. Explicitly, let  $\alpha \in (0, 1)$  be the confidence level, and we consider the following confidence interval of the relative score

$$\widehat{CI}(\alpha) := \left[ \hat{\delta}(\hat{\mathbb{P}}_1, \hat{\mathbb{P}}_2) - q_{1-\alpha/2} \sqrt{\frac{\hat{V}}{n_{test}}}, \hat{\delta}(\hat{\mathbb{P}}_1, \hat{\mathbb{P}}_2) + q_{1-\alpha/2} \sqrt{\frac{\hat{V}}{n_{test}}} \right], \quad (7)$$

where  $q_{1-\alpha/2}$  denotes the upper  $1 - \alpha/2$  quantile of a standard normal. The following statement establishes the validity of the confidence interval.

**Corollary 4.2.** *Under the conditions in Corollary 4.1, for any  $\alpha \in (0, 1)$ ,*

$$\mathbb{P} \left( \delta(\hat{\mathbb{P}}_1, \hat{\mathbb{P}}_2) \in \widehat{CI}(\alpha) \right) \xrightarrow{P} 1 - \alpha. \quad (8)$$

We remark that performing inference for the Wasserstein distance-based evaluation metrics is challenging due to its significant estimation bias and computational complexity. Additional details are provided in Appendix A.

## 5 Computation

In this section, we discuss the computation of  $\hat{p}_1(y)$  in our proposed estimator (5). By Proposition 2,

$$\log(\hat{p}_1(y)) = -\|g_1^{-1}(y)\|_2^2/2 - d_1 \log(\sqrt{2\pi}) + \log(|J_{g_1}|(g_1^{-1}(y))), \quad (9)$$

where we substitute the density of the multivariate normal distribution. Similarly, we obtain (9) for  $\log(\hat{p}_2(y))$ . Then the estimator  $\hat{\delta}(\hat{\mathbb{P}}_1, \hat{\mathbb{P}}_2)$  in (5) takes the form

$$\begin{aligned} & \frac{1}{n_{test}} \sum_{i=1}^{n_{test}} \frac{1}{2} (\|g_2^{-1}(Y_i)\|_2^2 - \|g_1^{-1}(Y_i)\|_2^2) + (d_2 - d_1) \log(\sqrt{2\pi}) \\ & + \log(|J_{g_1}|(g_1^{-1}(Y_i))) - \log(|J_{g_2}|(g_2^{-1}(Y_i))). \end{aligned} \quad (10)$$

For generative models used in practice such as auto-encoder or diffusion model,  $g_1^{-1}$  is typically represented as a neural network or a composition of multiple neural network transformations. Thus, the primary computational cost arises from evaluating the log determinant of the Jacobian matrix. Fortunately, our estimator (10) is well-suited for parallel computing, as  $\log(|J_{g_1}|(g_1^{-1}(Y_i)))$  and  $\log(|J_{g_2}|(g_2^{-1}(Y_i)))$  can be computed in parallel for all  $Y_i$ 's in the data set. In addition, if the Jacobian or its determinant is stored during the final epoch of training, it can be retrieved to compute the relative score approximately. In the following, we provide further details on computing  $\log(|J_{g_1}|(g_1^{-1}(Y_i))) - \log(|J_{g_2}|(g_2^{-1}(Y_i)))$ .

### 5.1 Jacobian determinant of function inverse

Since the Jacobian of the inverse function is the inverse matrix of the Jacobian of the original function, we have multiple equivalent forms for the term  $\log(|J_{g_1}|(g_1^{-1}(Y_i))) - \log(|J_{g_2}|(g_2^{-1}(Y_i)))$  in (10),

$$\begin{aligned} & \log(|J_{g_1}|(g_1^{-1}(Y_i))) - \log(|J_{g_2}|(g_2^{-1}(Y_i))) \\ & = -\log(|J_{g_1^{-1}}|(Y_i)) + \log(|J_{g_2^{-1}}|(Y_i)) \\ & = \log(|J_{g_1^{-1} \circ g_2}|(g_2^{-1}(Y_i))) \\ & = \log(|J_{g_2^{-1} \circ g_1}|(g_1^{-1}(Y_i))). \end{aligned}$$

Explicitly,  $\log(|J_{g_1^{-1}}|(Y_i))$  computes the log determinant of the Jacobian matrix of the inverse function  $g_1^{-1}$ , evaluated at the test data point  $Y_i$ ;  $\log(|J_{g_1^{-1} \circ g_2}|(g_2^{-1}(Y_i)))$  computes the log determinant of the composite function  $g_1^{-1} \circ g_2$ , evaluated at the latent embedding  $g_2^{-1}(Y_i)$  of the test data point under the second generative model. In practice, either of these equivalent formulations can be chosen based on which Jacobian determinants can be computed more efficiently and accurately.

As an example, in a diffusion model, the reverse process can be expressed as a composition of a sequence of denoising steps  $g_1 = g_{1,S} \circ g_{1,S-1} \circ \dots \circ g_{1,1}$  for some  $S \in \mathbb{N}$ . Using the multiplicative property of matrix determinants,  $|AB| = |A||B|$  for matrices  $A$  and  $B$ , the log determinant of the Jacobian for  $g_1$  can be written as

$$\log(|J_{g_1}|) = \sum_{s=1}^S \log(|J_{g_{1,s}}|).$$

This decomposition allows us to compute the Jacobian determinant for each individual denoising step  $g_{1,s}$ , take the logarithm, and sum them up. Typically, each denoising step involves a neural network transformation, and its Jacobian matrix can be computed using existing deep learning frameworks<sup>6</sup>. The determinant can then be computed using methods such as LU decomposition or the Bareiss algorithm.

## 6 Numerical analysis

We conduct experiments on both simulated and empirical datasets<sup>7</sup>. In Section 6.1, we use simulated examples to evaluate the finite-sample performance of our confidence intervals (7) and to empirically compare the coverage rates of our methods with other existing metrics for generative models. In Section 6.2, we illustrate our approach on CIFAR10 data using the Denoising Diffusion Implicit Model (Song, Meng, and Ermon 2021), comparing the performance of the DDIM model across different numbers of sampling steps.

### 6.1 Simulated data

We use  $\mathbb{P}, \hat{\mathbb{P}}_1, \hat{\mathbb{P}}_2$  to denote the distribution of  $Y, Y_1$ , and  $Y_2$  and generate the data by:

$$\begin{aligned} X, X_1, X_2 &\sim \mathcal{N}(0, I_d), \\ Y &\sim AX + B, \quad Y_1 \sim AX_1 + B, \quad Y_2 \sim (A + \epsilon I_d)X_2 + B + \epsilon, \end{aligned} \tag{11}$$

where  $d = 10$ ,  $A \in \mathbb{R}^{d \times d}$  is a constant diagonal matrix with diagonal elements generated from  $\text{Uniform}(0.8, 1.2)$ ,  $B \in \mathbb{R}^d$  is a constant vector generated from  $\mathcal{N}(0, I_d)$ , and  $\epsilon \in \mathbb{R}$  is a constant controls the difference between  $\hat{\mathbb{P}}_1$  and  $\hat{\mathbb{P}}_2$ . Then the generative models are defined by the transformations:  $g_1(X) = AX + B, g_1^{-1}(X) = A^{-1}(X - B), g_2(X) = (A + \epsilon I_d)X + B + \epsilon, g_2^{-1}(X) = (A + \epsilon I_d)^{-1}(X - B - \epsilon)$ . We consider  $\epsilon \in \{0.01, 0.02, \dots, 0.2\}$ , generate  $n = 1000$  sample from  $Y$ , and construct the confidence interval via (7) with  $\alpha = 0.1$ .

We compute the coverage rate and power of our confidence interval over 1000 repeated experiments. The results are shown in Figure 3. Our confidence intervals achieve coverage rates close to the target level. For comparison, we estimate  $-\text{KL}(\mathbb{P} \parallel \hat{\mathbb{P}}_1)$  and  $-\text{KL}(\mathbb{P} \parallel \hat{\mathbb{P}}_2)$  using a  $k$  nearest neighbor (kNN) based estimator (Zhao and Lai 2020) and construct confidence intervals for  $-\text{KL}(\mathbb{P} \parallel \hat{\mathbb{P}}_1) + \text{KL}(\mathbb{P} \parallel \hat{\mathbb{P}}_2)$  using resampling methods including Subsampling (Politis and Romano 1994) and Adaptive HulC (Kuchibhotla, Balakrishnan, and Wasserman 2024). We also examine the estimation and resampling-based inference of the Wasserstein-2 distance difference,  $-W_2^2(\mathbb{P}, \mathbb{P}_1) + W_2^2(\mathbb{P}, \mathbb{P}_2)$ , where each  $W_2$  distance is estimated using the empirical distributions. As shown in Figure 3, these methods fail to provide faithful confidence intervals for the KL divergence difference.

We further investigate why existing estimators fail to provide valid confidence intervals, we examine their distributions numerically. Figure 4 presents histograms of the estimators alongside the true values of relative KL divergence and relative  $W_2$  distance when  $\epsilon = 0.05$ . The results show that these estimators exhibit

<sup>6</sup>For instance, in PyTorch, it can be done with the function `TORCH.AUTOGRAD.FUNCTIONAL.JACOBIAN`, which automates the calculation of the Jacobian matrix for a given input.

<sup>7</sup>The codes of numerical analysis can be found at <https://github.com/sylydya>.

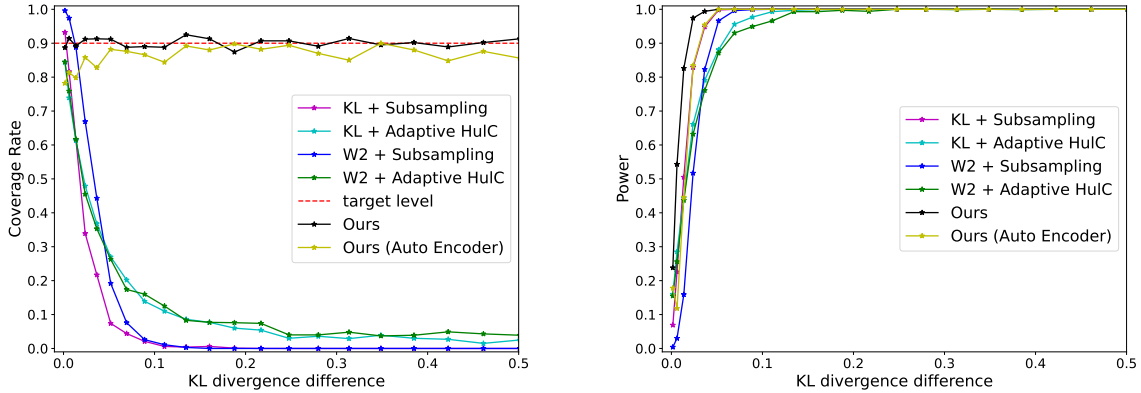


Figure 3: Coverage rate and power of confidence intervals constructed by our methods (7) and existing KL divergence and  $W_2$  distance estimator paired with resampling methods (Subsampling and Adaptive HulC).

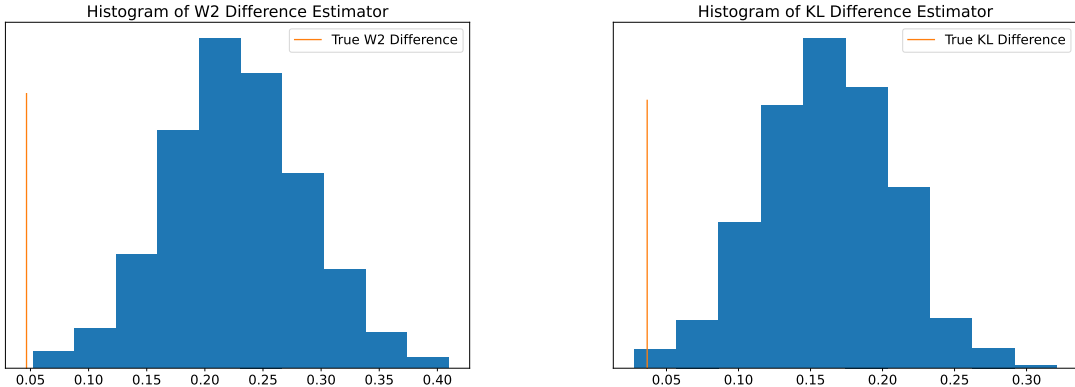


Figure 4: Histogram of the existing estimators of  $W_2$  distance and KL divergence. The vertical line indicates the true value for the simulated example.

significant bias, making them unsuitable for reliable inference. This empirical observation is consistent with our discussion of the challenges in estimating KL divergence and  $W_2$  distance (Section 3 and Appendix A).

**Auto-encoder.** We consider the case where the generator  $g$ 's inverse  $g^{-1}$  is not directly available. In this case, we can train an auto-encoder minimizing the reconstruction error using the data generated from  $g$ . The encoder can effectively serve as  $g^{-1}$ .

Explicitly, we consider the same data generation mechanism (11), and generate  $N = 5 \times 10^5$  samples from  $Y_1$  (from  $g_1$ ) and  $Y_2$  (from  $g_2$ ) and train two auto-encoders to reconstruct the data. Both the encoder and decoder are fully connected neural networks with a single hidden layer containing 100 units. The auto-encoders are trained for 20 epochs using the Adam optimizer (Kingma 2014). To enforce that the encoder maps the data to  $\mathcal{N}(0, 1)$ , we introduce a penalty term  $\text{KL}(\mathcal{N}(\hat{\mu}, \hat{\Sigma}) \parallel \mathcal{N}(0, I_d))$ , where  $\hat{\mu}$  and  $\hat{\Sigma}$  are the empirical mean and covariance matrix of the encoder outputs. We use the two learned encoders as  $g_1^{-1}$  and  $g_2^{-1}$ , respectively.

To assess the performance of our method, we again generate  $n = 1000$  samples from  $Y$ , compute the estimator in (10), and construct the confidence intervals using (7). The coverage rates over 1000 repeated experiments are summarized in Figure 3 (denoted as ‘‘Ours (Auto Encoder)’’). The results show that our

S	FID	$\widehat{CI}(\alpha)$ of $\delta(\hat{P}_S, \hat{P}_{100})$
20	6.84	(-39.91, -38.70)
50	4.67	(-17.40, -16.63)
100	4.16	-

Table 1: Comparison of DDIM model with different number of denoising steps  $S$ . In particular, we compare  $S = 20$  and  $S = 50$  over  $S = 100$ . A larger number of denoising steps  $S$  leads to a model with better FID scores and KL divergence. Our confidence interval doesn't cover 0, indicating  $\hat{P}_{100}$  is significantly better than both  $S = 20$  and  $S = 50$ .

method achieves coverage rates close to the target level, even when using the learned inverse functions.

## 6.2 Diffusion model

We apply our methods to real datasets: evaluating pre-trained Denoising Diffusion Implicit Models (Song, Meng, and Ermon 2021) on the CIFAR-10 dataset. We consider the deterministic forward pass (see e.g. Section 4.3 of Song, Meng, and Ermon 2021) as the inverse transformation of the generative model. To highlight the advantages of our approach, we consider similar diffusion models, where statistical inference is essential for demonstrating significant improvements. Specifically, we compare the DDIM model with different numbers of denoising steps,  $S = 20, 50, 100$ , and denote the corresponding generative distribution by  $\hat{P}_S$ . Following Song, Meng, and Ermon 2021, we select the sub-sequence time steps using the Quadratic schedule. The results are summarized in Table 1.

Our results are consistent with those of Song, Meng, and Ermon 2021 based on FID. Specifically, Song, Meng, and Ermon 2021 shows that DDIM models with a larger number of denoising steps  $S$  achieve better FID scores, our method also indicates that larger  $S$  results in lower KL divergence. Moreover, while the FID scores of  $\hat{P}_{50}$  and  $\hat{P}_{100}$  are similar, our results indicate that DDIM model with  $S = 100$  is significantly better.

## 7 Discussions

In this paper, we proposed a model-free and nuisance-free approach for quantitatively comparing generative models with statistical confidence. First, we propose focusing on the relative performance gap (relative score) between two generative models, rather than evaluating their absolute performances individually. Second, we developed an unbiased estimator for the relative score that achieves parametric convergence rates and is asymptotically normal, enabling rigorous inference. Third, on simulated datasets with known ground truth, our method effectively controls type I error while achieving comparable or superior power, whereas existing metrics often exhibit near-zero coverage; when applied to diffusion models on real image datasets without ground truth, our approach yields statistically confident conclusions consistent with FID.

We outline several promising directions for future research.

- Extension to the comparison of multiple generative models. Our estimator (5) of the relative score and its asymptotic distribution characterization Theorem 4.1 naturally extend to pairwise comparisons of multiple generative models. Combined with Fan et al. 2024, we can identify the best-performing model and establish the full ranking of multiple generative models with statistical confidence.
- Heterogeneity in relative performance. There may be significant heterogeneity in the relative performance of generative models across test datasets, e.g., a model that excels at generating cat images might perform poorly on car images. In future works, we aim to use our method to identify the strengths of different generative models with statistical confidence, which can further guide the development of expert models that strategically leverage the strengths of individual models for improved performance.
- Stopping time of training. In training, if the current model's performance does not show significant improvement over the model from the previous epoch, training should be stopped to prevent overfitting

and save computational resources. Our proposal allows for a statistically confident comparison between the current model and the previous epoch’s model, ensuring that the decision to stop training is based on rigorous and reliable evaluation criteria.

- Stochastic reverse processes. Extending our evaluation method to generative models with a non-deterministic reverse process where Assumption 2.2 does not hold, such as the Denoising Diffusion Probabilistic Models (DDPM) (Ho, Jain, and Abbeel 2020), would be an intriguing direction for future research.

## References

Achiam, Josh et al. (2023). “Gpt-4 technical report”. In: *arXiv preprint arXiv:2303.08774*.

Arizono, Ikuo and Hiroshi Ohta (1989). “A test for normality based on Kullback—Leibler information”. In: *The American Statistician* 43.1, pp. 20–22.

Belov, Dmitry I and Ronald D Armstrong (2011). “Distributions of the Kullback–Leibler divergence with applications”. In: *British Journal of Mathematical and Statistical Psychology* 64.2, pp. 291–309.

Chen, Ricky TQ et al. (2018). “Neural ordinary differential equations”. In: *Advances in neural information processing systems* 31.

Chong, Min Jin and David Forsyth (2020). “Effectively unbiased fid and inception score and where to find them”. In: *Proceedings of the IEEE/CVF conference on computer vision and pattern recognition*, pp. 6070–6079.

Del Barrio, Eustasio and Jean-Michel Loubes (2019). “Central limit theorems for empirical transportation cost in general dimension”. In: *The Annals of Probability* 47.2, pp. 926–951.

Dinh, Laurent, Jascha Sohl-Dickstein, and Samy Bengio (2016). “Density estimation using real nvp”. In: *arXiv preprint arXiv:1605.08803*.

Dümbgen, Lutz (1993). “On nondifferentiable functions and the bootstrap”. In: *Probability Theory and Related Fields* 95.1, pp. 125–140.

Fan, Jianqing et al. (2024). “Ranking inferences based on the top choice of multiway comparisons”. In: *Journal of the American Statistical Association*, pp. 1–14.

Goodfellow, Ian et al. (2014). “Generative adversarial nets”. In: *Advances in neural information processing systems* 27.

Heusel, Martin et al. (2017). “Gans trained by a two time-scale update rule converge to a local nash equilibrium”. In: *Advances in neural information processing systems* 30.

Ho, Jonathan, Ajay Jain, and Pieter Abbeel (2020). “Denoising diffusion probabilistic models”. In: *Advances in neural information processing systems* 33, pp. 6840–6851.

Karras, Tero et al. (2020). “Analyzing and improving the image quality of stylegan”. In: *Proceedings of the IEEE/CVF conference on computer vision and pattern recognition*, pp. 8110–8119.

Kingma, Diederik P (2013). “Auto-encoding variational bayes”. In: *arXiv preprint arXiv:1312.6114*.

— (2014). “Adam: A method for stochastic optimization”. In: *arXiv preprint arXiv:1412.6980*.

Kuchibhotla, Arun Kumar, Sivaraman Balakrishnan, and Larry Wasserman (2024). “The HulC: confidence regions from convex hulls”. In: *Journal of the Royal Statistical Society Series B: Statistical Methodology* 86.3, pp. 586–622.

Panaretos, Victor M and Yoav Zemel (2019). “Statistical aspects of Wasserstein distances”. In: *Annual review of statistics and its application* 6.1, pp. 405–431.

Politis, Dimitris N and Joseph P Romano (1994). “Large sample confidence regions based on subsamples under minimal assumptions”. In: *The Annals of Statistics*, pp. 2031–2050.

Rezende, Danilo and Shakir Mohamed (2015). “Variational inference with normalizing flows”. In: *International conference on machine learning*. PMLR, pp. 1530–1538.

Salimans, Tim et al. (2016). “Improved techniques for training gans”. In: *Advances in neural information processing systems* 29.

Song, Jiaming, Chenlin Meng, and Stefano Ermon (2021). “Denoising diffusion implicit models”. In: *International Conference on Learning Representations*.

Song, Yang and Stefano Ermon (2019). “Generative modeling by estimating gradients of the data distribution”. In: *Advances in neural information processing systems* 32.

Vaart, Aad W Van der (2000). *Asymptotic statistics*. Vol. 3. Cambridge university press.

Van Den Oord, Aäron, Nal Kalchbrenner, and Koray Kavukcuoglu (2016). “Pixel recurrent neural networks”. In: *International conference on machine learning*. PMLR, pp. 1747–1756.

Van Den Oord, Aaron et al. (2016). “Wavenet: A generative model for raw audio”. In: *arXiv preprint arXiv:1609.03499* 12.

Villani, Cédric et al. (2009). *Optimal transport: old and new*. Vol. 338. Springer.

Zhao, Puning and Lifeng Lai (2020). “Minimax optimal estimation of KL divergence for continuous distributions”. In: *IEEE Transactions on Information Theory* 66.12, pp. 7787–7811.

## A Literature

### A.1 Dissimilarity metrics between distributions

We include a brief review of two types of metrics for quantifying the dissimilarity between distributions. The definitions of the two types of metrics have been introduced in the main text, and we include the definitions here for completeness.

#### A.1.1 f-divergence

The first metric is the f-divergence. For a convex function  $f : [0, +\infty) \rightarrow (-\infty, +\infty]$  such that  $f(x)$  is finite for all  $x > 0$ ,  $f(1) = 0$ , and  $f(0) = \lim_{t \rightarrow 0^+} f(t)$ , the f-divergence of  $P$  from  $Q$  is given by

$$D_f(\mathbb{P} \parallel \hat{\mathbb{P}}_1) \equiv \int_{\Omega} f\left(\frac{p(y)}{\hat{p}_1(y)}\right) \hat{p}_1(y) dy$$

KL-divergence is a special case of f-divergence with  $f(x) = x \log(x)$ .

Estimating f-divergence typically requires the estimation of two densities,  $p$  and  $\hat{p}_1$ , where the estimation of  $p$  exposes us to the curse of dimensionality. For the associated relative score, according to Proposition 1, the nice cancellation that simplifies computation is unique to the KL-divergence. Consequently, for divergences other than KL, the estimation of  $p$  becomes unavoidable.

#### A.1.2 Wasserstein-p distance

Wasserstein- $p$  distance (Villani et al. 2009) is defined as

$$W_p(\mathbb{P}, \hat{\mathbb{P}}_1) = \inf_{\gamma \in \Gamma(\mathbb{P}, \hat{\mathbb{P}}_1)} \mathbb{E}_{(x,y) \sim \gamma}^{1/p} [\|x - y\|_p^p],$$

where  $\Gamma(\mathbb{P}, \hat{\mathbb{P}}_1)$  is the set of all couplings of  $\mathbb{P}$  and  $\hat{\mathbb{P}}_1$ .

We discuss the challenges of performing inference for evaluation methods based on the Wasserstein- $p$  distance. Del Barrio and Loubes 2019 shows that<sup>8</sup>

$$\sqrt{n} \left( W_2^2(\mathbb{P}_n, \hat{\mathbb{P}}_{1,n}) - \mathbb{E}[W_2^2(\mathbb{P}_n, \hat{\mathbb{P}}_{1,n})] \right) \xrightarrow{w} \mathcal{N}(0, \sigma^2(\mathbb{P}, \hat{\mathbb{P}}_1)),$$

where the asymptotic variance  $\sigma^2(\mathbb{P}, \hat{\mathbb{P}}_1)$  can be estimated consistently using a plug-in estimator. The issue is that the center  $\mathbb{E}[W_2^2(\mathbb{P}_n, \hat{\mathbb{P}}_{1,n})]$  is different from the desired  $W_2^2(\mathbb{P}, \hat{\mathbb{P}}_1)$ , and the gap between  $\mathbb{E}[W_2^2(\mathbb{P}_n, \hat{\mathbb{P}}_{1,n})]$  and  $W_2^2(\mathbb{P}, \hat{\mathbb{P}}_1)$  scales as  $n^{-1/d}$  (Villani et al. 2009). In addition, for the relative Wasserstein-2 distance  $W_2^2(\mathbb{P}, \hat{\mathbb{P}}_1)$ , the joint asymptotic distribution of  $(W_2^2(\mathbb{P}_n, \hat{\mathbb{P}}_{1,n}), W_2^2(\mathbb{P}_n, \hat{\mathbb{P}}_{2,n}))$  is required. It remains unclear whether  $W_2^2(\mathbb{P}_n, \hat{\mathbb{P}}_{1,n})$  and  $W_2^2(\mathbb{P}_n, \hat{\mathbb{P}}_{2,n})$  are asymptotically jointly Gaussian, as well as the exact form of their covariance matrix<sup>9</sup>. Subsampling methods (Dümbgen 1993) can be employed for conducting inference for Wasserstein- $p$  distances; however, subsampling is computationally expensive, especially given that the Wasserstein- $p$  distance is already difficult to compute. For a comprehensive review of these issues, see Panaretos and Zemel 2019.

<sup>8</sup>CLT results of general Wasserstein- $p$  distance are largely unknown.

<sup>9</sup>The off-diagonal values of the covariance matrix is non-zero because both  $W_2^2(\mathbb{P}_n, \hat{\mathbb{P}}_{1,n})$  and  $W_2^2(\mathbb{P}_n, \hat{\mathbb{P}}_{2,n})$  depend on  $\mathbb{P}_n$ .

## A.2 Existing evaluation metrics of generative models

We describe the inception score (IS) (Salimans et al. 2016) and the Frechet Inception Distance (FID) (Heusel et al. 2017), two most commonly used quantitative scores for generative models. We note that these metrics were originally designed for training GANs rather than for model evaluation, with more emphasis placed on computational efficiency than on statistical rigor.

IS evaluates the quality of a generative model by applying a separate, pretrained image classification model to a batch of images generated by the model. IS is maximized when the classifier confidently predicts a single label for each image, or when the predictions are evenly distributed across all possible labels. The quality of IS depends heavily on the quality of the classifier (if the classifier consistently outputs a single label for all images, the IS becomes uninformative). Another disadvantage is that IS does not compare generated images to test images.

FID compares the distribution between the distribution of test images and that of generated images. Mathematically, FID is defined as the Wasserstein-2 distance between the two distribution. However, the Wasserstein-2 distance is computationally expensive for random vectors, except for multivariate Gaussians. To approximate the FID, the default approach involves two steps: (1) mapping the real and generated images to  $\mathbb{R}^d$  separately by passing them through the final layer of an image classifier to extract essential features; (2) fitting multivariate Gaussian distributions to the transformed data in  $\mathbb{R}^d$  and computing the Wasserstein-2 distance between these multivariate Gaussians. The approximation accuracy depends on how well the transformation to  $\mathbb{R}^d$  captures the data characteristics and the quality of the multivariate Gaussians fit to the transformed data (the covariance matrix is typically not diagonal and the estimation involves  $O(d^2)$  elements). Chong and Forsyth 2020 shows that FID could be significantly biased in finite sample.

## B Proofs

*Proof of Proposition 1.* For simplicity, we use  $\mathbb{P}_1$  instead of  $\hat{\mathbb{P}}_1$ ,  $p_1$  instead of  $\hat{p}_1$ , and similarly for  $\mathbb{P}_2$  and  $p_2$ . For any densities  $p(x)$ ,  $p_1(x)$ ,  $p_2(x)$ , we define

$$h(p, p_1, p_2) := \int f\left(\frac{p_1(x)}{p(x)}\right) - f\left(\frac{p_2(x)}{p(x)}\right) p(x) dx.$$

For any  $\delta(x)$  such that  $\int \delta(x) dx = 0$ , and  $t$  such that  $p(x) + t\delta(x) \geq 0$ , by the calculus of variations and Eq. (4),

$$\begin{aligned} \int g(p_1(x), p_2(x)) \delta(x) dx &= \frac{\partial}{\partial t} h(p + t\delta, p_1, p_2) |_{t=0} \\ &= \int \left( -f'\left(\frac{p_1(x)}{p(x)}\right) \frac{p_1(x)}{p^2(x)} + f'\left(\frac{p_2(x)}{p(x)}\right) \frac{p_2(x)}{p^2(x)} \right) \delta(x) p(x) dx \\ &\quad + \int \left( f\left(\frac{p_1(x)}{p(x)}\right) - f\left(\frac{p_2(x)}{p(x)}\right) \right) \delta(x) dx \\ &= \int -f'\left(\frac{p_1(x)}{p(x)}\right) \frac{p_1(x)}{p(x)} \delta(x) + f'\left(\frac{p_2(x)}{p(x)}\right) \frac{p_2(x)}{p(x)} \delta(x) \\ &\quad + f\left(\frac{p_1(x)}{p(x)}\right) \delta(x) - f\left(\frac{p_2(x)}{p(x)}\right) \delta(x) dx. \end{aligned} \tag{12}$$

We let  $f_1(x) = f(e^x)$ , then  $f_1(\log(x)) = f(x)$  and  $f'_1(\log(x)) \cdot (1/x) = f'(x)$ , which implies  $f'_1(\log(x)) = xf'(x)$ . We replace  $f(x)$  by  $f_1(x)$  in Eq. (12),

$$\begin{aligned} \int g(p_1(x), p_2(x)) \delta(x) dx &= \int \left( -f'_1\left(\log\left(\frac{p_1(x)}{p(x)}\right)\right) + f_1\left(\log\left(\frac{p_1(x)}{p(x)}\right)\right) \right. \\ &\quad \left. + f'_1\left(\log\left(\frac{p_2(x)}{p(x)}\right)\right) - f_1\left(\log\left(\frac{p_2(x)}{p(x)}\right)\right) \right) \delta(x) dx. \end{aligned} \tag{13}$$

Since Equation (13) is true for arbitrary  $\delta(x)$  such that  $\int \delta(x) = 0$ , then we let  $f_2(x) = -f'_1(x) + f_1(x)$  and have

$$g(p_1(x), p_2(x)) = f_2(\log(p_1(x)) - \log(p(x))) - f_2(\log(p_2(x)) - \log(p(x))) + C, \quad \forall x. \quad (14)$$

for some constant  $C \in \mathbb{R}$ . We assume  $C = 0$ , otherwise, we replace  $g(p_1(x), p_2(x))$  by  $g(p_1(x), p_2(x)) - C$ . Note that  $f_2(0) = -f'_1(0) + f_1(0) = -f'_1(0) + f(1) = -f'_1(0)$ . We let  $f_3(x) = f_2(x) + f'_1(0)$ , then  $f'_3(0) = 0$  and  $g(p_1(x), p_2(x)) = f_3(\log(p_1(x)) - \log(p(x))) - f_3(\log(p_2(x)) - \log(p(x)))$ . Take  $p(x) = p_1(x)$  in Eq. (14),

$$g(p_1(x), p_2(x)) = f_3(0) - f_3(\log(p_2(x)) - \log(p_1(x))) = f_3(\log(p_2(x)) - \log(p_1(x))). \quad (15)$$

We let  $a = \log(p_2(x)) - \log(p_1(x))$ ,  $b = \log(p(x)) - \log(p_2(x))$ , then by Eq. (15),

$$f_3(a + b) - f_3(b) = f_3(a). \quad (16)$$

Since  $f \in C^1$ , then  $f_3$  is continuous. By the result of Cauchy's functional equation, there exists  $c, d \in \mathbb{R}$  such that

$$f_3(x) = cx + d, \quad \forall x. \quad (17)$$

By the definition of  $f_3(x)$  and Eq. (17), we have  $f_2(x) = f_3(x) - f'_1(0) = cx + d'$  for some  $d' \in \mathbb{R}$ . By the definition of  $f_2(x)$ ,

$$-f'_1(x) + f_1(x) = cx + d'.$$

This is a standard ODE problem, and we multiply both sides by  $e^{-x}$  to get

$$\begin{aligned} - (e^{-x} f_1(x))' &= cxe^{-x} + d'e^{-x} \\ \implies e^{-x} f_1(x) &= -cxe^{-x} - ce^{-x} - d'e^{-x} + d'' \\ \implies f_1(x) &= \alpha e^x + \beta x + \theta, \end{aligned}$$

where  $d'', \alpha, \beta, \theta \in \mathbb{R}$ . By the definition of  $f_1(x)$ ,  $f(x) = \alpha x + \beta \log(x) + \theta$ . Note that  $f(1) = 0$ , which implies  $\alpha + \theta = 0$ . Note that  $\int (\alpha(d\mathbb{P}_1/d\mathbb{P}) - \alpha)d\mathbb{P} = 0$ , therefore, the divergence with  $f(x) = \alpha x + \beta \log(x) + \theta$  is the same as that of  $\beta \log(x)$ . Since  $f(x)$  is convex, we have  $\beta \leq 0$ , and we finish the proof.  $\square$

*Proof of Proposition 2.* By Assumption 2.1 with Gaussian noise distribution,  $Z_1 := g_1^{-1}(Y) \stackrel{d}{=} \mathcal{N}(0, I_{d_1})$  for  $Y \sim \hat{P}_1$ . By the change of measure,

$$\hat{p}_1(y) = \hat{q}_1(z_1) \cdot |J_{g_1}|(z_1) = \phi_{d_1}(g_1^{-1}(y)) \cdot |J_{g_1}|(g_1^{-1}(y)). \quad (18)$$

$\square$

*Proof of Proposition 3.* Proposition 3 follows from the linearity of expectation and the fact that the test data  $Y_i \sim \mathbb{P}$ .  $\square$

*Proof of Theorem 4.1.* Recall that  $Y_i$  are i.i.d. sampled from  $\mathbb{P}$ . Theorem 4.1 is an application of the Lindeberg-Lévy central limit theorem to i.i.d. random variables  $\log(\hat{p}_1(Y_i)) - \log(\hat{p}_2(Y_i))$ .  $\square$

*Proof of Corollary 4.1.* When  $0 < V < \infty$ , by the law of large numbers of i.i.d. random variables, the empirical variance  $\hat{V}$  of  $\log(\hat{p}_1(Y_i)) - \log(\hat{p}_2(Y_i))$  converges to  $V$  in probability. We further combine Slutsky's theorem and Corollary 4.1 to arrive at Theorem 4.1.  $\square$

*Proof of Corollary 4.2.* Corollary 4.2 comes from the definition of convergence in distribution and Corollary 4.1.  $\square$

## C Additional Algorithms

### C.1 DDIM

The log of the Jacobian determinant can be expressed as the sum of  $S$  (total number of iterations in the sampling process) sub log-Jacobian determinants, with each term corresponding to the transformation in one iteration. In each iteration, the transformation is given by,

$$x_{s-1} = \underbrace{\sqrt{\alpha_{s-1}} \left( \frac{x_s - \sqrt{1-\alpha_s} \epsilon_\theta^{(s)}(x_s)}{\sqrt{\alpha_s}} \right)}_{\sqrt{1-\alpha_{s-1}} \cdot \epsilon_\theta^{(s)}(x_s)}, \quad (19)$$

for a sequence of  $\alpha_s \in (0, 1)$ . To compute the Jacobian determinant for this transformation, it suffices to compute the Jacobian of  $\epsilon_\theta^{(s)}$ . Since  $\epsilon_\theta^{(s)}$  is parameterized by a U-Net architecture, its Jacobian can be directly read from the trained U-Net.

The reverse of the sampling process, which encodes a test image into latent noise, can be achieved by simulating the reverse of an ODE. In fact, DDIM can be considered as an Euler method to solve ODEs. Specifically, the iterative formula can be represented as

$$\sqrt{\frac{1}{\bar{\alpha}_{s-1}}} x_{s-1} - \sqrt{\frac{1}{\bar{\alpha}_s}} x_s = \left( \sqrt{\frac{1}{\bar{\alpha}_{s-1}}} - \sqrt{\frac{1}{\bar{\alpha}_s}} \right) \epsilon_\theta(x_s, s), \quad (20)$$

We set  $y_s := \sqrt{\frac{1}{\bar{\alpha}_s}} x_s$  and  $p_s := \sqrt{\frac{1}{\bar{\alpha}_s}} - 1$ ,

$$y_{s-1} - y_s = (p_{s-1} - p_s) \epsilon_\theta(x_s, s). \quad (21)$$

In the limit of small steps, this equation becomes an ODE:

$$dy_s = \epsilon_\theta(x_s, s) dp_s. \quad (22)$$

Then, the reversal of this ODE can be derived as follows:

$$y_{s+1} - y_s = (p_{s+1} - p_s) \epsilon_\theta(x_s, s), \quad (23)$$

which becomes,

$$\sqrt{\frac{1}{\bar{\alpha}_{s+1}}} x_{s+1} - \sqrt{\frac{1}{\bar{\alpha}_s}} x_s = \left( \sqrt{\frac{1}{\bar{\alpha}_{s+1}}} - \sqrt{\frac{1}{\bar{\alpha}_s}} \right) \epsilon_\theta(x_s, s). \quad (24)$$

## D Additional Experiments

We apply our methods to subsets of CIFAR-10 data set. Specifically, we compare the DDIM model with different numbers of denoising steps  $S = 50, 100$ . We construct the confidence interval (7) using images with the same label from the data set. Effectively, we are estimating  $\delta(\hat{\mathbb{P}}_{50}, \hat{\mathbb{P}}_{100}) = -\text{KL}(\mathbb{P} \parallel \hat{\mathbb{P}}_{50}) + \text{KL}(\mathbb{P} \parallel \hat{\mathbb{P}}_{100})$ , where  $\mathbb{P}$  corresponds to the distribution of images with certain label. Figure 5 shows the confidence interval computed using 4 different classes of images.

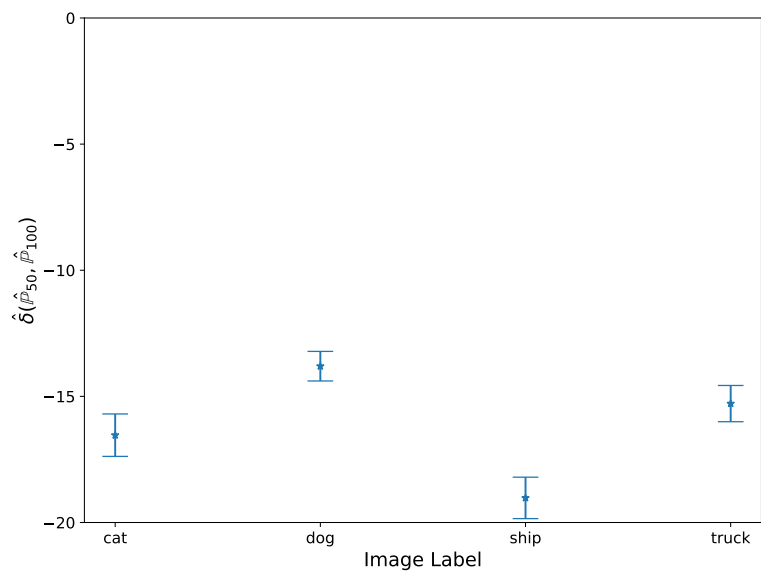


Figure 5: Confidence Interval for comparing DDIM mdoel with denoising steps  $S = 50$  ( $\hat{P}_{50}$ ) and  $S = 100$  ( $\hat{P}_{100}$ ).